

Chemistry in a gravitationally unstable protoplanetary disc

J. D. Ilee^{1*}, A. C. Boley², P. Caselli¹, R. H. Durisen³, T. W. Hartquist¹ and J. M. C. Rawlings⁴

¹*School Of Physics & Astronomy, University Of Leeds, Leeds LS2 9JT, UK*

²*Department of Astronomy, University of Florida, 211 Bryant Space Science Center, PO Box 112055, USA*

³*Department of Astronomy, Indiana University, 727 East 3rd Street, Swain West 319, Bloomington, IN 47405, USA*

⁴*Department of Physics & Astronomy, University College London, London WC1E 6BT, UK*

Accepted 2011 July 15. Received 2011 July 4; in original form 2011 May 1

ABSTRACT

Until now, axisymmetric, α -disc models have been adopted for calculations of the chemical composition of protoplanetary discs. While this approach is reasonable for many discs, it is not appropriate when self-gravity is important. In this case, spiral waves and shocks cause temperature and density variations that affect the chemistry. We have adopted a dynamical model of a solar-mass star surrounded by a massive ($0.39 M_{\odot}$), self-gravitating disc, similar to those that may be found around Class 0 and early Class I protostars, in a study of disc chemistry. We find that for each of a number of species, e.g. H_2O , adsorption and desorption dominate the changes in the gas-phase fractional abundance; because the desorption rates are very sensitive to temperature, maps of the emissions from such species should reveal the locations of shocks of varying strengths. The gas-phase fractional abundances of some other species, e.g. CS, are also affected by gas-phase reactions, particularly in warm shocked regions. We conclude that the dynamics of massive discs have a strong impact on how they appear when imaged in the emission lines of various molecular species.

Key words: stars: pre-main-sequence, stars: circumstellar matter, protoplanetary discs, astrochemistry

1 INTRODUCTION

In the last several years, the Plateau de Bure Interferometer (Dutrey et al. 2007; Henning et al. 2010) and the Submillimeter Array (Qi et al. 2008) have provided images of protoplanetary discs in an increasing variety of molecular line emissions. The field will be advanced further by the completion of the Submillimeter Array Disc Imaging Survey (Öberg et al. 2010). It will be revolutionised through the use of the Atacama Large Millimetre/submillimetre Array (ALMA), which will allow much weaker lines to be investigated, and thus will enable the characterisation of a more diverse range of processes (Guilloteau & Dutrey 2008; Semenov et al. 2008).

Many authors (e.g., Aikawa et al. 1999, 2002; Markwick et al. 2002; Bergin et al. 2003; Gorti & Hollenbach 2004; Ilgner et al. 2004; Nomura & Millar 2005; Willacy et al. 2006; Willacy 2007; Nomura et al. 2009; Woitke et al. 2009; Walsh et al. 2010; Fogel et al. 2011; Heinzeller et al. 2011) have pre-

sented computational results for the chemical composition of protoplanetary discs. Because α -disc models were adopted, these studies are relevant to protoplanetary discs that transport mass locally, both instantaneously and averaged in time, and by extension, to discs that possess global axisymmetry. For this reason, α -disc models may be inappropriate during early phases of gas accretion on to protoplanetary discs if discs become massive enough to trigger gas phase gravitational instabilities (GIs) (Vorobyov & Basu 2005, 2006, 2009; Boley 2009). GIs produce dynamic nonaxisymmetric structure in the form of spiral waves leading to shocks (see Durisen et al. 2007, for a review) and possibly, under some conditions, to bound protoplanetary fragments (Boss 2001; Mayer et al. 2004, 2007; Stamatellos et al. 2007; Boley et al. 2010; Vorobyov & Basu 2010; Boley & Durisen 2010). Fragmentation conditions are still under debate (see, e.g., Boss 2007; Cai et al. 2010; Podolak et al. 2010; Meru & Bate 2011; Lodato & Clarke 2011) but, for non-fragmenting cases, it is generally agreed that gravitational torques caused by spiral waves lead to significant mass transport (Gammie 2001;

* E-mail: pyjdi@leeds.ac.uk

Lodato & Rice 2004; Mejía et al. 2005; Boley et al. 2006, 2007a; Cossins et al. 2009; Michael et al. 2011).

Such mass transport may have implications for disc driven outbursts and recent, successful models for FU Orionis outbursts have been developed for the assumption that GIs dominate mass transport outside disc radii of a few AU in non-fragmenting discs (Armitage et al. 2001; Zhu et al. 2009, 2010). Simulations (Zhu et al. 2010) including layered accretion in the Dead Zone (Gammie 1996) as well as transport by GIs show that, when discs accrete from rapidly rotating cloud cores, disc masses can become comparable to those of their central stars. Simple α -disc models for disc evolution overlook the episodic heating induced by GI spiral shocks in massive discs (Boley & Durisen 2008). These shocks can cause desorption of volatiles from dust grains and can trigger gas-phase chemical reactions that would not otherwise occur. Both effects can produce observable chemical signatures of disc dynamics.

In this paper, we present results from a chemical model of a massive, young protoplanetary disc in which GIs cause the formation of spiral waves. Section 2 outlines the physical and chemical models we have utilised, and the assumed initial conditions. Section 3 contains results for the time-dependent fractional abundances within an individual fluid element and column density maps of the entire disc for different species. A comparison of results from this model with those of other models of disc chemistry are also given. Finally, Section 4 presents conclusions based on the results and comments on further avenues of research.

2 METHODS

2.1 The dynamical model

We use a hydrodynamic simulation of a massive ($0.39 M_{\odot}$) protoplanetary disc as the basis for the physical input to our chemical model. Most of the mass in the disc initially extends from a radial distance $r \sim 7$ to 50 au from the central, solar-mass protostar. The system represents an early Class I object, which would likely evolve into an F-type main sequence star. The disc is modelled with CHYMERA (Boley 2007), which solves the equations of hydrodynamics with self-gravity on a fixed, cylindrical Eulerian grid. The computational domain has 256, 128 and 64 zones in r , ϕ and z , respectively, with a physical resolution of $\Delta r = \Delta z = 0.25$ au. Mirror symmetry about the midplane is assumed. All grid boundaries have outflow conditions allowing mass to leave the global disc simulation, where the inner boundary is set to approximately 4 au, but no mass is allowed to enter. The central star is allowed to move freely, and the equation of motion for it is integrated as described in Boley (2009). We use the Boley et al. (2007b) equation of state with a fixed ortho-to-para ratio of hydrogen molecules of 3:1 (which is only relevant for the evolution of the physical model). The fractional mass abundances of hydrogen, helium and more massive elements are set to $X = 0.73$, $Y = 0.25$, and $Z = 0.02$, respectively. Because the hydrogen is almost entirely in H_2 , the mean molecular weight is 2.33 amu. For cooling, we use the radiative cooling approximation described in Boley (2009). An incident radiation field on the disc is assumed to have a black body spectrum with a temperature

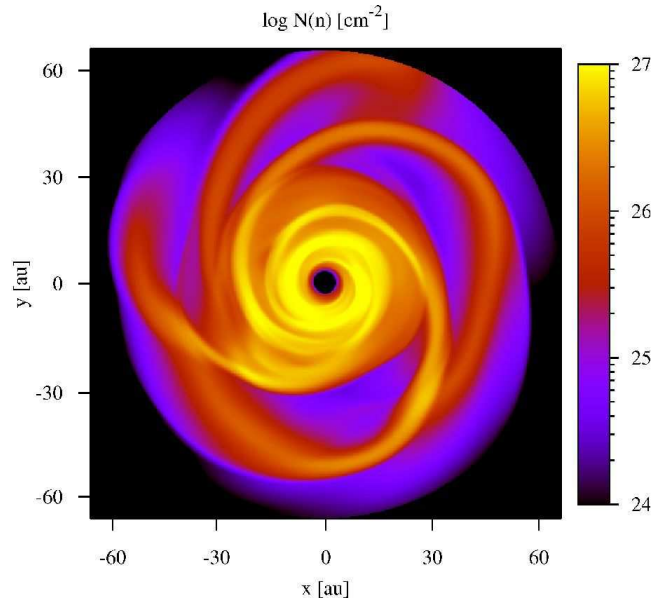


Figure 1. Column density of nuclei (see Eqn. 1 for the relationship between number density and mass density) in the disc viewed from above at the end of the simulation, $t = 388$ yr.

varying as $T_{\text{irr}} = 140(r/\text{au})^{-0.5} + 10$ K to account for heating by the star.

The initial disc model is prepared using the method described in Boley & Durisen (2008). An analytic disc model is first created, with a Toomre (1964) $Q \sim 1$ for most of the disc. The spiral instability sets in around $Q \sim 1.7$ (Durisen et al. 2007), so the initial model represents conditions before a strong burst of gravitational instabilities, as might be expected during the earliest stages of disc evolution. A flat Q profile with the irradiation law noted above requires the surface density to follow, roughly, $\Sigma \propto r^{-1.75}$. This initial configuration is assumed to undergo Keplerian rotation and have an adiabatic index of 5/3. These assumptions about the initial rotation and value of the adiabatic index can lead to large radial oscillations at the start of the simulation due to the associated deviations from equilibrium. To avoid some of this behavior, we evolve the analytic model in CHYMERA at low azimuthal resolution (8 zones) for 500 yr, which is about two orbital periods near $r \sim 45$ au. When the disc is loaded on to the higher resolution grid, a 5% cell-to-cell random noise is added to the density distribution, which seeds the growth of nonaxisymmetric structure. This is considered to be the time $t = 0$ in the initial disc. The disc is then run at higher azimuthal resolution for an additional 388 yr. Figure 1 shows the column density of nuclei for the disc viewed from above at the end of the simulation.

At the start of the full simulation ($t = 0$), 1000 fluid elements are randomly distributed throughout the disc, weighted by mass. These fluid elements are evolved along with the main simulation, and their thermal histories are recorded, as described in Boley & Durisen (2008). The division of the disc into more fluid element would have allowed the capture of rare events such as shocks that are atypically strong for the radii at which they occur. This would lead to slightly greater average gas phase abundances of species that are hard to desorb. However, this would not affect our overall

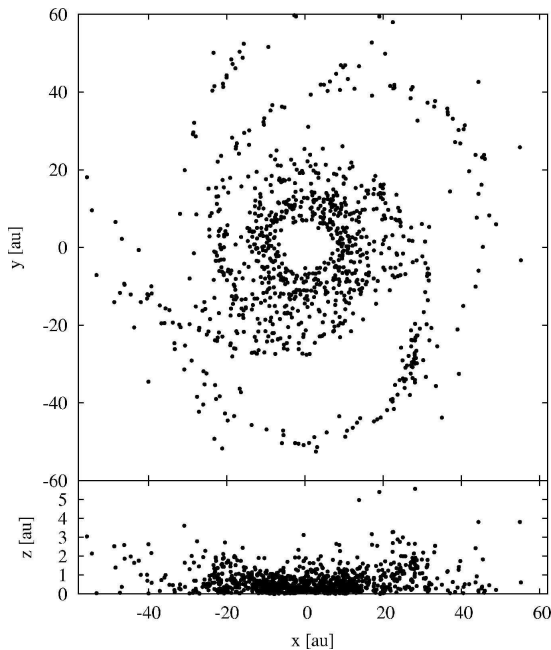


Figure 2. The final location of the fluid elements used to sample the disc, at $t = 388$ yr.

conclusions. By the end of the simulation, 5 fluid elements were lost through grid boundaries, leaving 995 elements with complete thermal histories. 963 of these were used to study the chemical evolution in the disc. Results for 16 of the 32 remaining fluid elements were not used to generate chemical results because the jump, for each of those 16, in the physical conditions from those at the end of the dynamical calculation back to those at the start of the dynamical calculation created difficulties for the integration of the chemical rate equations. Results for the other 16 were not used because spiked extrema in them caused problems for the chemical integration. These extrema occurred at temperatures of around 30 K - 40 K. The 32 elements were randomly distributed at the end of the simulation, and had not passed through shocks near the end of the dynamical calculation, so their influence on the chemical results was negligible. Figure 2 shows the distribution of the final locations of the fluid elements used in the chemical modelling.

Figure 3 shows the maximum line-of-sight temperature and the mass-averaged temperature $T_n = (\int nT dz) / (\int n dz)$ along the line-of-sight for a face-on view of the final disc. Here n is the number density of nuclei (see Eqn. 1), T is the temperature and dz is an infinitesimal path length along the line-of-sight. The maximum and mass-weighted line-of-sight temperatures were calculated from the full hydrodynamic model results, rather than from the properties of the massive fluid elements used in the chemical calculations, because the full hydrodynamic model results provide higher spatial resolution.

The spiral structure is clearly seen in the maximum line-of-sight temperature map. The structure is also seen in the mass-averaged temperature map, but is somewhat less sharply defined. The difference in the maps is due to the high temperature region being somewhat, but not highly, limited in extent. It lies near the midplane and contains only a fraction of the disc mass.

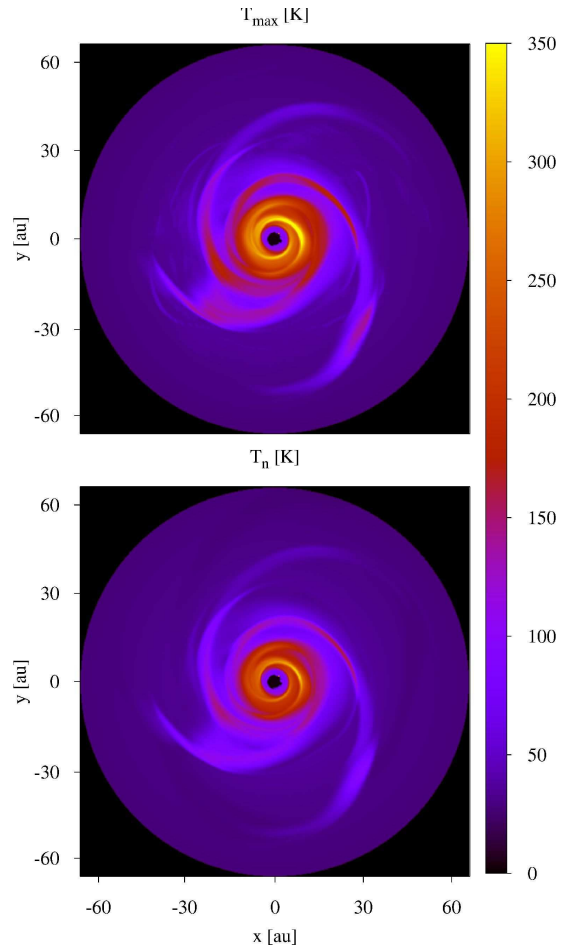


Figure 3. Maximum line of sight temperature (top) and mass averaged temperature (bottom) of the disc at $t = 388$ yr.

Figure 4 shows results, taken from the complete hydrodynamical data, for the temperature and number density of nuclei in planes containing the rotation axis and either the North-South axis (y) or the East-West axis (x) from Fig. 2. The temperature is less than 150 K outside the inner 20 au of the disc, while within it, the temperature can reach up to 350 K. The number density plot shows that the highest density gas lies in a ring-like structure at approximately 10 au from the centre.

The temperature and density histories of the fluid elements shown in Fig. 2 form the physical input to the chemical model. Figure 5 shows the evolution of the temperature and density of one of the fluid elements. This element begins at 0.8 au above the midplane, approximately 30 au from the centre of the disc. It follows a nearly circular path that slowly increases in radius. After one-and-a-half orbits, or 270 yr, it encounters the first shock. Both shocks do not affect the circular motion, but instead cause the element to rise to approximately 1.8 au above the midplane. The results for this track provide a useful example, because the fluid element experiences a relatively quiescent period for 270 yr, before encountering the shocks. These shocks rapidly raise the temperature to a maximum of 140 K and the number density to 10^{13} cm^{-3} . The temperature and density appear to peak at the same time and drop together. This is due

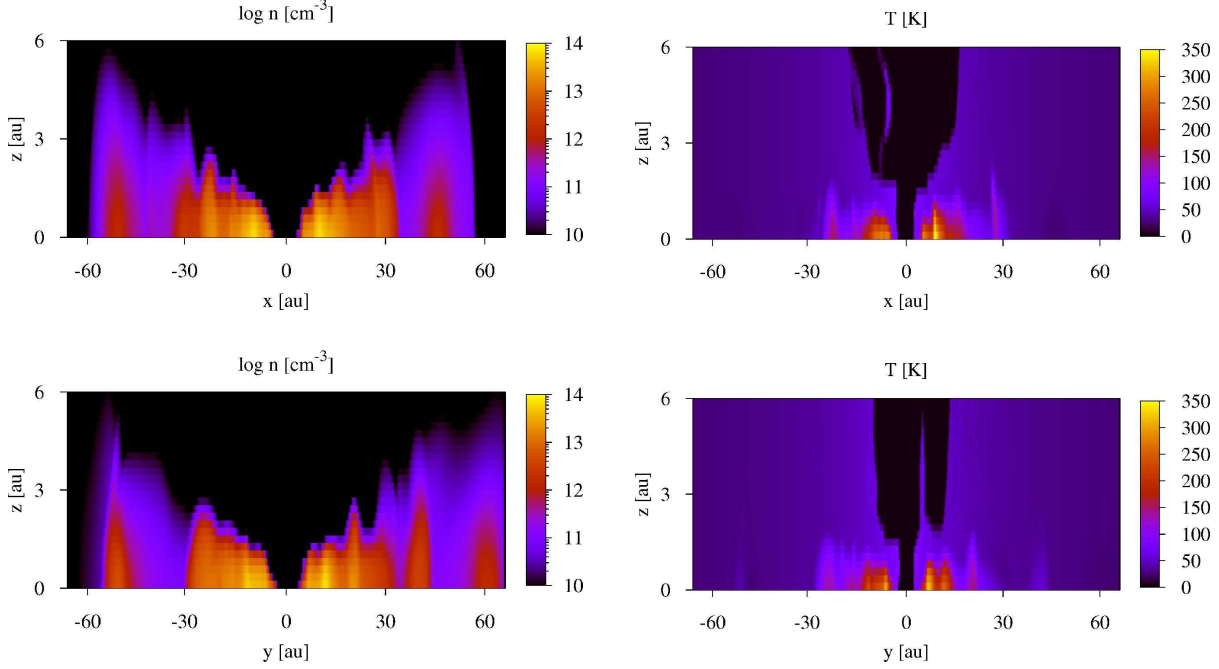


Figure 4. Slices of the disc interior showing number densities and temperatures at $t = 388$ yr. The x -axis here corresponds to a slice along the x -axis of Fig. 1 where $y = 0$, and vice versa.

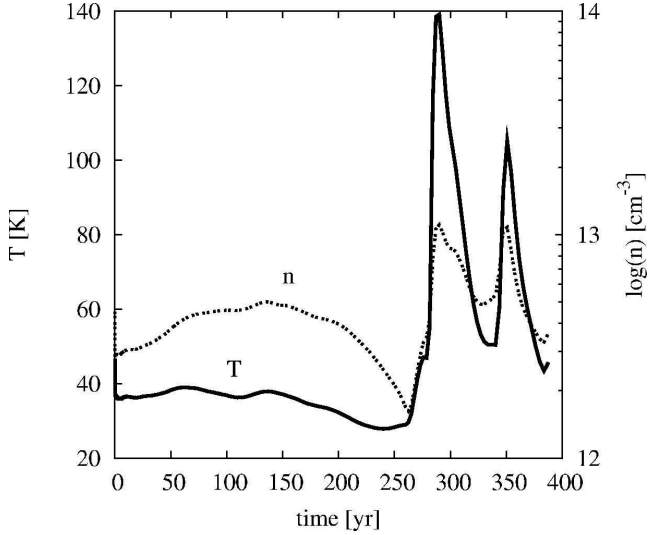


Figure 5. Temperature and number density history of a fluid element from the disc. This particular element encounters a shock at about 270 and 350 yr.

to the increase in the pressure caused by a shock driving an expansion of gas parallel to the shock and obliquely to the mid-plane of the disc that begins almost immediately behind the shock (see Boley & Durisen 2008).

2.2 The chemical model

The chemical computation is based on a network of rate equations involving 1334 reactions and 125 species containing the elements H, He, C, O, N, Na and S. These reactions were originally selected from a subset of the UMIST

Rate 95 database (Millar et al. 1997). Data from the Kinetic Database For Astrochemistry, KIDA¹, were used to update some of the rates and rate coefficients. Thermal desorption processes (discussed in detail below) and some three-body reactions (see Appendix B) were added to the network.

At each time-step in the chemical network, the temperature and mass density of each fluid element are derived with cubic spline fits to the data provided for the element from the physical model. These interpolated values of the temperature and mass density are then used in the time-integration of the rate equations. The number density of nuclei, n , is calculated from the mass density, ρ , by

$$n = \frac{N_A}{M} \rho = n_H + n_{He} + n_Z, \quad (1)$$

where n_H , n_{He} and n_Z are the number densities of hydrogen, helium and more massive nuclei, respectively. We have assumed a molar mass of $M = 1.28 \text{ g mol}^{-1}$, which is appropriate for a relative abundance of helium-to-hydrogen of 0.09 with trace amounts of more massive elements. Integrations were performed with the DVODE package (Brown et al. 1989) to obtain the fractional abundance, $X(i) = n(i)/n$, of each species.

The rate equation for the gas-phase fractional abundance of the i th species is

$$\frac{d}{dt} X(i) = \sum_{j,l,m} k(j) X(l) X(m) n - \sum_{j',m} k(j') X(i) X(m) n - 2 \sum_{j''} k(j'') X(i)^2 n - \Gamma_{cr}(i) X(i) + S_3(i) + S_{a,d}(i), \quad (2)$$

where $k(j)$ is the rate coefficient of the j th reaction and the summations are restricted so that only reactions involved

¹ <http://kida.obs.u-bordeaux1.fr>

in the formation or removal of the i th species are included. $\Gamma_{\text{cr}}(i)$ is the rate at which direct cosmic-ray ionisation and cosmic-ray-induced photoemission remove species i . $S_3(i)$ and $S_{\text{a,d}}(i)$ are source terms due to three-body reactions and adsorption on to and desorption from grain surfaces, respectively. We assume that the only third body of importance is H_2 , an assumption which introduces only an insignificant error. Thus,

$$S_3(i) = \sum_{j,l,m} k(j)X(l)X(m)X(\text{H}_2)n^2 \quad (3)$$

$$- \sum_{j',m} k(j')X(i)X(m)X(\text{H}_2)n^2$$

$$- 2 \sum_{j''} k(j'')X(i)^2X(\text{H}_2)n^2.$$

2.2.1 Rate coefficients and rates

Here we present a brief summary of the forms of the gas-phase rate coefficients and rates that we have adopted. More detail can be found in the primary paper on the UMIST Rate 95 database (Millar et al. 1997). The reaction rates and coefficients that we use are provided online².

The rate coefficient for the j th two- or three-body reaction is of the standard Arrhenius form

$$k(j) = \alpha(j) \left(\frac{T}{300} \right)^{\beta(j)} \exp \left(\frac{-\gamma(j)}{T} \right), \quad (4)$$

where $\alpha(j)$ is the room temperature rate coefficient of the reaction (at 300 K), $\beta(j)$ describes the temperature dependence and $\gamma(j)$ is the activation energy of the reaction.

The rate for the destruction of species i due to cosmic rays is given by

$$\Gamma_{\text{cr}}(i) = a(i)\zeta + \frac{\zeta P(i)}{1-A}, \quad (5)$$

where $a(i)$ is a proportionality constant, $\zeta = 10^{-17} \text{ s}^{-1}$ is the cosmic ray ionisation rate, $P(i)$ is a constant and A is the dust grain albedo, which we take to be 0.5. Because the two terms on the right represent the physically distinct processes of direct cosmic ray induced ionisation and of destruction due to photoemission induced by the collisions of molecular hydrogen with energetic electrons produced by the ionisation, data tables give $a(i)$ and $P(i)$ separately.

Though photoabsorption of radiation from external sources will affect the chemistry in the outer layers of a disc, we focus on the bulk of the disc material and assume that it is well shielded from external sources of photons. Thus, we neglect photoabsorption, other than that of cosmic-ray-induced photoemission.

2.2.2 Gas-grain reactions

With minor exceptions, we assume that no surface chemistry occurs, though we recognise that surface chemistry is important in establishing the chemical initial conditions that we adopt. The exceptions concern the neutralisation of ions, which we assume occurs when they are adsorbed. While studies of the chemistry of discs including

surface reactions and grain evolution have been performed (Schreyer et al. 2008; Henning et al. 2010; Semenov et al. 2010; Vasyunin et al. 2011; Semenov & Wiebe 2011), such chemistry remains very uncertain. This is why we have assumed that the initial abundances reflect those of cometary ices (see Section 2.3).

$S_{\text{a,d}}(i)$ has contributions due to adsorption and desorption, and we take

$$S_{\text{a,d}}(i) = S_{\text{d}}(i) - S_{\text{a}}(i), \quad (6)$$

where

$$S_{\text{a}} = \pi a^2 S(i) \eta \sqrt{\frac{8kT}{\pi \mu m_{\text{H}}}} X(i) n. \quad (7)$$

The sticking coefficient $S(i)$ is set to unity, and we take the ratio of the number density of dust grains to the number density of nuclei to be $\eta = 3.3 \times 10^{-12}$, which is appropriate for a dust grain radius and grain-to-gas mass ratio of about $a = 0.1 \mu\text{m}$ and 0.01, respectively. T_{g} is the gas temperature, k is the Boltzmann constant, μ is the molecular mass in amu and m_{H} is the mass of a hydrogen atom.

We treat thermal desorption in the same way as Visser et al. (2009), and

$$S_{\text{d}}(i) = 1.26 \times 10^{-21} (\sigma/\text{cm}^{-2}) f(i) \nu_0(i) \exp \left(\frac{-E_{\text{b}}(i)}{k T_{\text{d}}} \right), \quad (8)$$

where σ is surface density of binding sites, which we take to be $1.5 \times 10^{15} \text{ cm}^{-2}$. $E_{\text{b}}(i)$ is the binding energy of the i th species on the surface of the dust grain, T_{d} is the dust temperature (which we assume to be in equilibrium with T_{g}), the factor $f(i)$ represents the fraction of the surface of the dust grain covered by the i th species, given by

$$f(i) = \min \left(1, \frac{X^{\text{s}}(i)}{\eta N_{\text{b}}} \right), \quad (9)$$

where $X^{\text{s}}(i)$ is the solid fractional abundance of the i th species and N_{b} is the typical number of binding sites per grain, taken to be 10^6 . The characteristic vibrational frequency of the species attached to the grain is given by

$$\nu_0(i) = \sqrt{\frac{2\sigma E_{\text{b}}(i)}{m(i)\pi^2}}, \quad (10)$$

where $m(i)$ is the mass of the i th species (Hasegawa et al. 1992). The binding energies were taken from Hollenbach et al. (2009), references therein, and the OSU database³.

2.3 Chemical initial conditions

The initial gas-phase fractional abundances were assumed to have the same ratios to one another as the fractional abundances of the corresponding ices in comet Hale-Bopp as given by Ehrenfreund & Charnley (2000), and they are given in Table 1. Because comets are thought to have undergone significant chemical processing at the edges of discs, this assumption may not be entirely appropriate. However, comparisons between the compositions of cometary ices and interstellar ices imply a general consistency between the two,

² <http://www.ast.leeds.ac.uk/~pyjdi/chemdisc/network.txt>

³ <http://www.physics.ohio-state.edu/~eric/research.html>

Table 1. Initial fractional abundances ($X(i) = n(i)/n_{\text{H}}$). Note that $a(b) \equiv a \times 10^b$.

Species	Abundance	Species	Abundance
He	1.00(-1)	H ₂ CO	1.83(-6)
C	3.75(-4)	CO ₂	3.67(-5)
CO	3.66(-5)	HCN	4.59(-7)
CH ₄	1.10(-6)	HNC	7.34(-8)
N	1.15(-4)	S	1.62(-5)
NH ₃	3.30(-6)	H ₂ S	2.75(-6)
O	6.74(-4)	SO	1.47(-6)
H ₂ O	1.83(-4)	SO ₂	1.84(-7)
Na	3.50(-5)	OCS	3.30(-6)

though some discrepancies exist (Ehrenfreund & Charnley 2000; Ehrenfreund & Schutte 2000).

2.4 Timescales

As mentioned above, the hydrodynamical simulation following the disc evolution is run at higher resolution for 388 yr. This is far longer than the orbital period of about 4 yr at the inner boundary and somewhat shorter than the orbital period of 390 yr at 60 au. Nearly all of the mass is at less than 50 au where the period is about 300 yr, and the gravitational instability develops fully and leads to well established spiral structure in about 200 yr. The spiral structure roughly co-rotates with the material between about 30 and 40 au; the orbital period at 35 au is 180 yr. The disc is not steady, and the mass infall rate varies with radius and time from a factor of a few smaller than to a factor of a few larger than $10^{-4} \text{ M}_{\odot}$, which implies a radial flow time of the order of 10^4 yr. These timescales are much longer than the shortest chemical timescales which are associated with adsorption and desorption; using Eqn. 7, one finds that the adsorption timescale for a number density of 10^{13} cm^{-3} is roughly an hour. The desorption timescale is very much larger or smaller, depending on the temperature.

388 yr is sufficient to allow the spiral shocks to develop fully. This disc is already exhibiting spiral structure that is typical in GI-active discs over many orbits. The purpose of the hydrodynamical simulation is to provide self-consistent shock profiles for the chemical model, which was achieved in a relatively short period of evolution.

We follow the chemistry of each fluid element through ten cycles of the temperature and number density history associated with it (e.g., the history shown in Fig. 5), where in each subsequent cycle, we used the final fractional abundances from the previous cycle as initial input. Of course, this resulted in rapid variations in the physical conditions, as each new cycle began. However, we followed the chemical evolution in this way to keep the amount of data produced by the model at manageable levels. We found that the chemical behaviour for a fluid element became periodic by the time that the chemistry had gone through ten cycles. All results presented here are from the final cycle, and $t = 0$ occurs at the beginning of that cycle.

At the start of each integration, we used a logarithmically increasing time-step, which was initially 90 s. This allowed initially rapid reactions, such as the adsorption of species on to grains at the beginning of the first cycle, to be

followed with sufficient resolution. We limited the maximum time-step to approximately 10^3 s to avoid missing details in rapidly changing shock features.

3 RESULTS

The main results of the paper are column density maps for a variety of gas-phase species. To obtain them, we followed the chemical evolution of each fluid element. Before presenting the column density maps, we consider the chemistry in one fluid element as an illustrative example of the effect of shocks on the chemistry of the material.

3.1 An individual fluid element

Figure 6 shows the fractional abundances of 17 species (CO, SO, NH₃, H₂O, H₂S, OCS, O₂, HCO, HCO⁺, HNO, SO₂, CS, HCS, HCS⁺, HCN, HNC and OCN) as functions of time during the final cycle for the fluid element for which the density and temperature are given as functions of time in Fig. 5. The shocks induce increases in the gas-phase fractional abundances of all 17 species. However, the increase in $X(\text{CO})$ is too small to be apparent from the figure, because nearly all CO is in the gas-phase even in the coldest regions of the disc.

The increases of the fractional abundances of species for which results are shown in the upper two right hand panels are due almost entirely to thermal desorption from the surfaces of dust grains. We define $N_{\text{g}}(i)$ to be the average number of molecules of the i th species on a grain. For each species for which results are given in those panels, $N_{\text{g}}(i)\eta + X(i)$ is nearly constant. This is due to adsorption and desorption being the only processes significantly affecting the gas-phase fractional abundances of these species, and the fractional abundance of each of them depends almost entirely on the temperature only.

The fractional abundances of species for which results are shown in the other panels are affected significantly by gas-phase reactions, as well as desorption and adsorption. The higher temperatures in the shocks allow some reactions with activation energies and some endothermic reactions to occur at significant rates. Also species which undergo reactions that are exothermic and have small or no barriers are desorbed into the gas-phase in shocked regions.

HCS is one species having a fractional abundance that is affected by gas phase reactions. It is formed by the reaction of S and CH₂. CS is formed by reactions of C with SO, and S with CN in almost equal proportions. OCN is formed by the reaction of CN and O₂. HNO forms by the reaction of NH₂ and O, and HCO forms mainly via NH₃⁺ reacting with H₂CO. The reaction of O with OH contributes to O₂ production throughout much of the disc; O₂ is also formed in the shocked regions by the reactions of He⁺ with CO₂ and SO₂.

3.2 The entire disc

A major aim of the work reported here is the identification of the general features that should appear in images of gravitationally unstable protoplanetary discs obtained in molecular

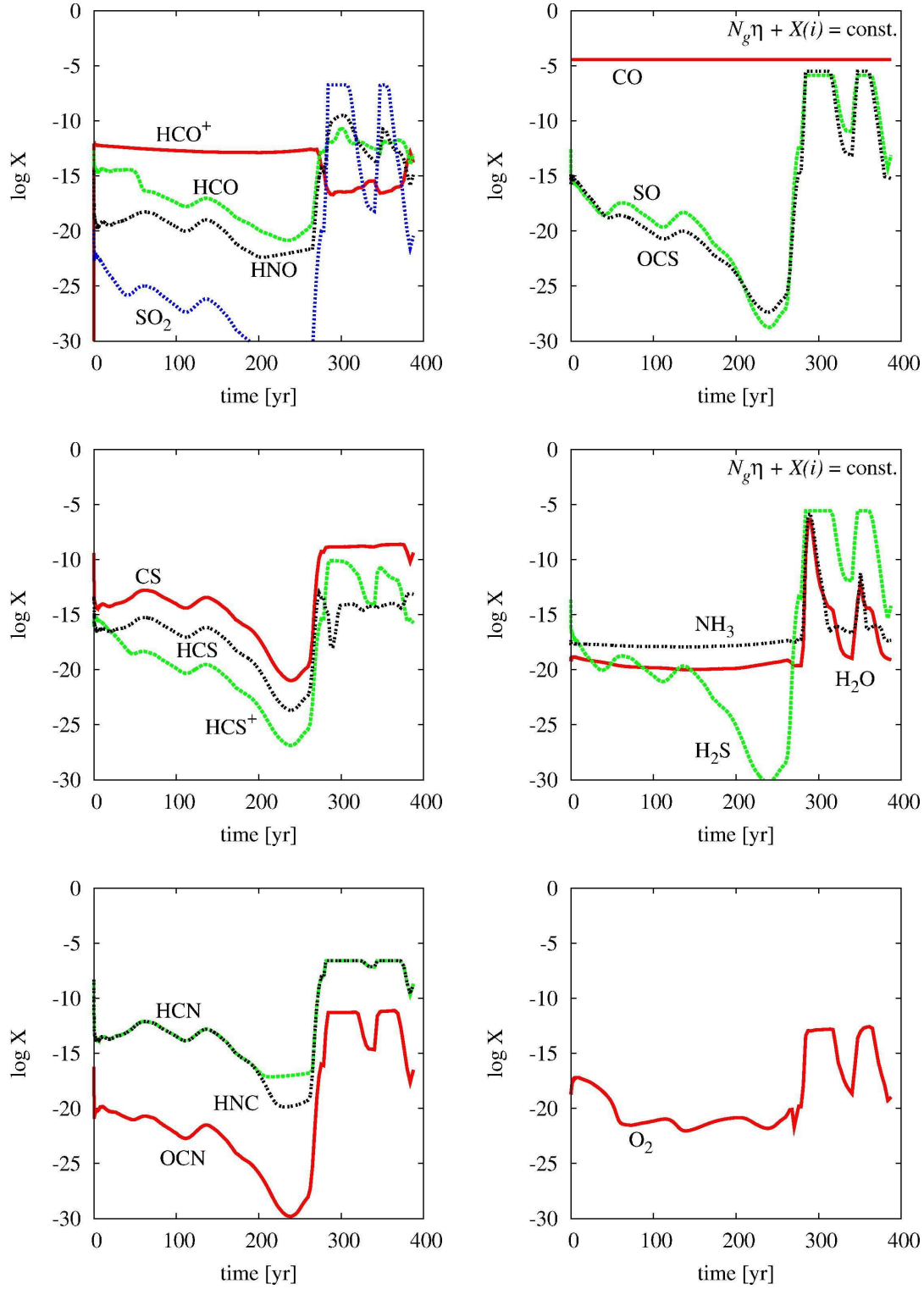


Figure 6. Fractional abundances of species as functions of time for the fluid element for which the physical structure is shown in Fig. 5. The relatively cold, quiescent period for the first 270 yr shows the abundance of most species decreasing due to adsorption, or staying constant.

line emissions. Thus, we present model column density maps for a number of molecular species.

The final spatial positions of the fluid elements constitute an irregular grid for which the model fractional abundances are known. The QHULL and QGRID3 interpolation rou-

tines contained within the IDL 5.5 libraries were used to obtain the fractional abundances at the points of a three-dimensional regular Cartesian grid. The mass density at each of those grid points was calculated from the mass density distribution at the final time given by the full hydrody-

namic results. We used the mass density distribution given by the full fluid results because the grid for which it was calculated is much more uniform than the grid for which the chemical results are available. Thus, for regions of low mass density, we were able to obtain more accurate interpolated results for the mass density than for the fractional abundances.

The column density $N(i, x, y)$ of the i th species on a line of sight perpendicular to the disc is

$$N(i, x, y) = \int nX(i, x, y, z) dz. \quad (11)$$

We assumed that n and all $X(i, x, y, z)$ s are even functions of z when performing the integrals. Figures 7 and 8 show the column densities of selected species. For each species for which results are given in Fig. 7, $N_g(i)\eta + X(i)$ is nearly constant. This is due to adsorption and desorption being the only processes significantly affecting the gas-phase fractional abundances of these species. Thus, the structure seen in each of these column densities is due to the variations in temperature and density and is not influenced by gas-phase chemistry.

$N_g(i)\eta + X(i)$ is not constant for each of the species for which Fig. 8 shows a gas-phase column density map. Gas-phase chemistry significantly affects the gas-phase fractional abundance of each of these species. We have already given some explanation for the evolution of most of the species for which results are displayed in Fig. 8 in Section 3.1. The HCO^+ is anticorrelated with the H_2O and other species with which it charge exchanges. HCS^+ is also removed by charge exchange with H_2O , but its distribution differs somewhat from that of HCO^+ . This is due to CS being abundant in the gas-phase only in regions in which it is efficiently desorbed and CO being abundant everywhere in the disc. Reactions of H_3^+ with CS and CO produce these ions.

3.3 The effect of three-body reactions

The chemistry in each of several fluid elements was calculated both with the three-body reactions included and with them excluded. As expected, the largest differences occur in the denser inner regions of the disc and spiral arms. Even there, the effects were insignificant for all species except some with low fractional abundances ($X(i) < 10^{-10}$).

A reduction of the fractional abundance of O_2 in one element from approximately 10^{-14} to 10^{-21} in a shocked region and an enhancement in the fractional abundance of NH from approximately 10^{-17} to 10^{-14} were amongst the most pronounced effects of including the three-body reactions. Species with fractional abundances higher than approximately 10^{-10} were not noticeably affected by the addition of the three-body reactions. The results that we present were obtained with the three-body reactions included.

3.4 Comparison with other models

The three-dimensional nature of our chemical model and the qualitatively different dynamics of the disc make a direct comparison of our results with the previously existing chemical results for axisymmetric models of lower mass discs difficult. However, we give a rough comparison between the maximum fractional abundances of species given by our model

Table 2. Maximum abundances reported in this work, W2010 and I2004. A dash signifies no data for that species were available in the original paper.

Species i	Maximum log $X(i)$		
	This work	W2010	I2004
HCO^+	-10.8	-6	-14
HCN	-6.4	-6.5	-
CN	-7.8	-7.5	-
CS	-8.0	-8	-10
C_2H	-10.5	-7	-
H_2CO	-5.7	-9	-
N_2H^+	-19.6	-11	-
H_2O	-3.7	-4	-
CO_2	-4.5	-4.5	-
OH	-12.8	-4	-14
S	-9.9	-	-15
SO	-5.8	-	-10
SO_2	-6.5	-	-7
HCS^+	-12.5	-	-21
NH_3	-5.5	-	-5

and some obtained by others who have investigated chemistry for disc models. The results taken from the other papers are somewhat inaccurate because they were obtained through the examination of figures from which precise information was hard to infer. Table 2 shows the maximum fractional abundances recorded at the end of our simulation and the corresponding values from Walsh et al. (2010) and Ilgner et al. (2004) (hereafter W2010 and I2004 respectively). Our results are comparable to those of the other models for NH_3 , SO_2 , H_2O , CO_2 , CN, CS and HCN. We obtain a higher fractional abundance of HCO^+ than I2004, but less than reported in W2010. Our fractional abundances of C_2H and N_2H^+ are lower than those of W2010. However, we report a much higher fractional abundance of H_2CO .

Some of the discrepancies between the results of W2010 and I2004 arise because W2010 considered a much more extensive fraction of the disc than I2004 who studied only the material at radii less than 10 au. We studied material at radii between 10 and 60 au, where spiral structure and shocks are important in our dynamical model. Thus, in further discussion of the differences between our results and those of others, we focus on a comparison of our results and those of W2010.

Some of these differences are due to the assumptions that we made concerning the initial chemical conditions. As mentioned earlier, in our model a number of species have gas-phase abundances that depend only on the assumed initial conditions and the balance between desorption and absorption. H_2CO in particular is such a species. So its high abundance in our model compared to that found by W2010 is due to our assumption of a higher H_2CO abundance and neglect of species as massive as CH_3OH . Similarly, our assumption that no nitrogen is initially in N_2 leads to a lower abundance of N_2H^+ than W2010 found.

The high values of the HCO^+ and C_2H given for W2010 occur in regions with densities that are about four orders of magnitude lower than any that we consider; these regions have correspondingly lower total column densities than the much denser regions do and in the W2010 model, the chemistry in them is affected by the diffusion that W2010 assume

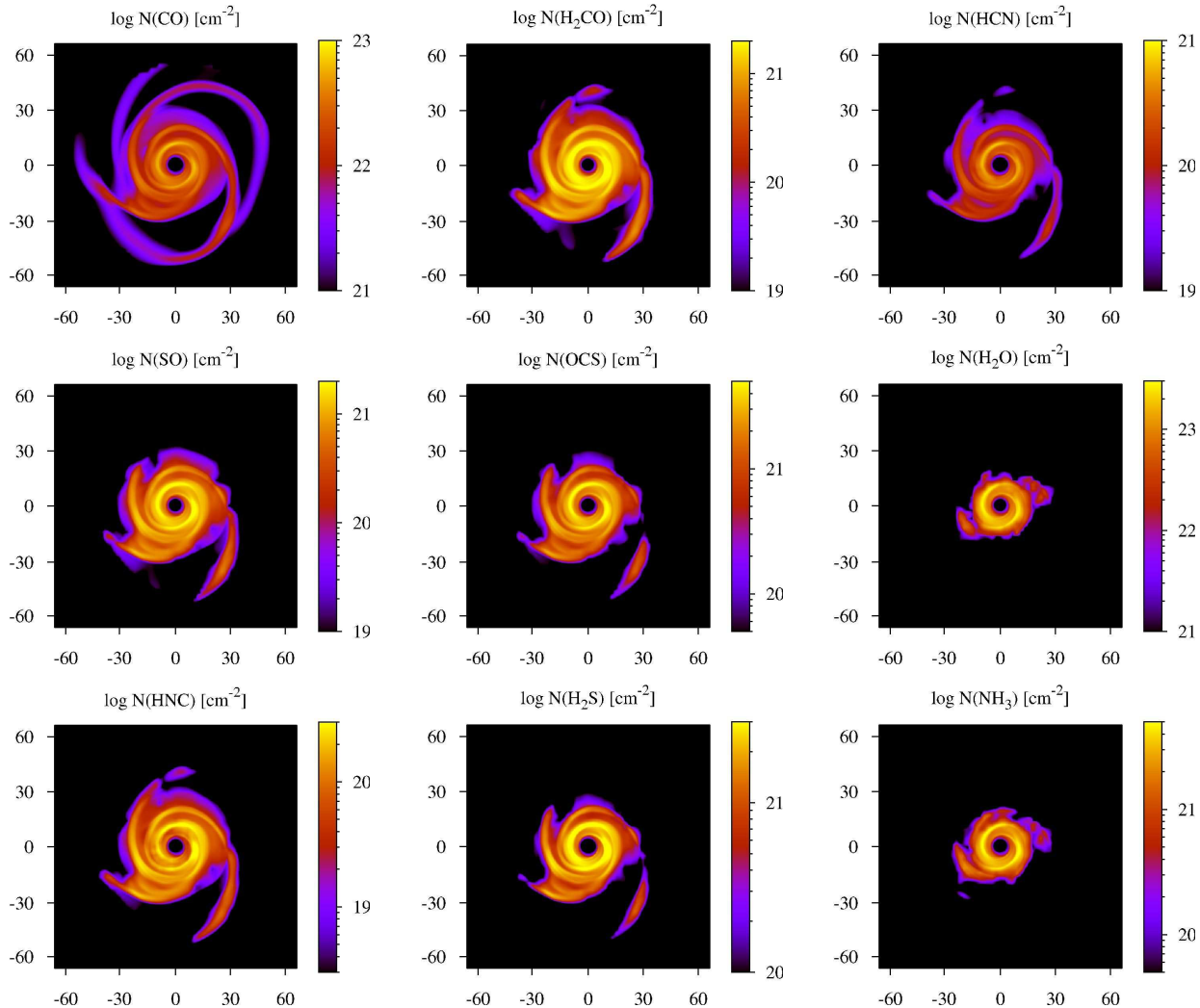


Figure 7. gas-phase column densities of molecules having gas-phase fractional abundances determined primarily by desorption and adsorption, at $t = 388$ yr. Distances from the disc centre are in au.

to occur, but which we do not. The mid-plane value obtained by W2010 for the fractional abundance of HCO⁺ for radii of 10 to 60 au is comparable to the maximum value that we report for it; this is to be expected because in both models most of the CO is in the gas phase, and HCO⁺ is formed by a simple ionisation triggered reaction sequence. The mid-plane value obtained by W2010 for the fractional abundance of C₂H for radii of 10 to 60 au is less than the maximum value that we report for it; this is due to the desorption, caused by shock induced heating, occurring near the mid-plane in our models.

4 CONCLUSIONS & FUTURE WORK

We have constructed a chemical model of a 0.39 M_⊙ protoplanetary disc, surrounding a solar-mass star, representative of a Class 0 or early Class I system. In the disc, gravitational instabilities cause spiral waves. The shocks associated with these waves induce the desorption of various chemical species from the surface of dust grains and increase their gas-phase abundances. Though the gas-phase fractional abundances

of some of the species are not significantly affected by gas-phase chemistry, some of the desorbed species are reactive. In some cases, the elevated temperatures in the shocked regions enhance the reactivity.

Because most of the mass is concentrated in spiral structures, all of the gas-phase molecular column densities show spiral structures. However, the structures are limited in extent in some species, e. g. H₂O, which possess the highest binding energies to grains, therefore higher temperatures are needed for desorption to occur. This also limits the extent of structure in species which form in the gas-phase from these tightly bound species. Consequently, maps of the emissions of a number of species will reveal where shocks of differing strengths are and, thus, serve as diagnostics of the disc dynamics.

We find that three-body reactions have little effect on the chemistry of species with fractional abundances above 10^{-10} . Though they are most important in the hotter, densest regions of the disc, they do not alter the overall chemistry of the disc significantly.

A direct comparison of our results with those of other models is not straightforward, due largely to the very differ-

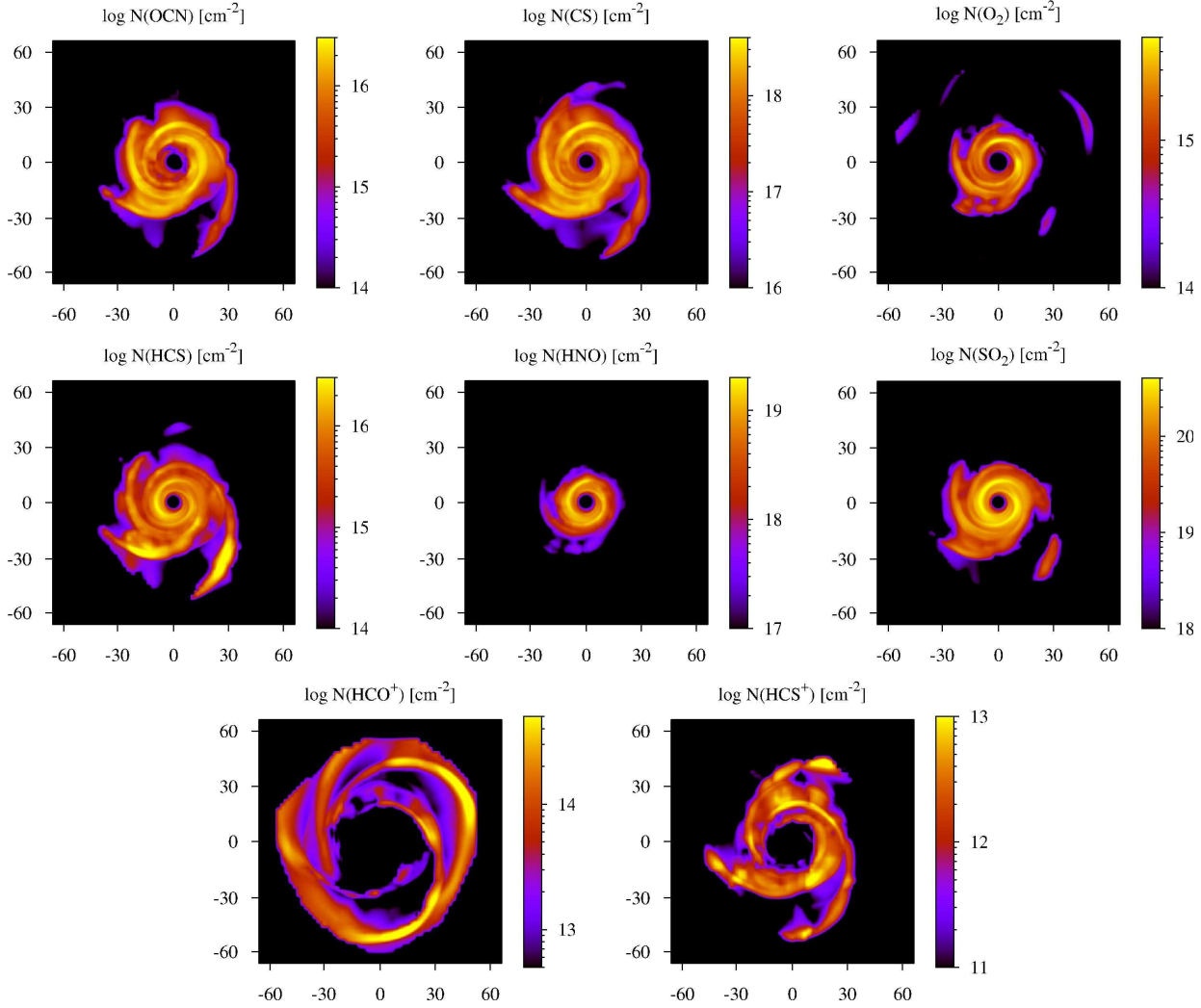


Figure 8. Column densities in the disc for several gas-phase molecules whose total abundance varies with time, at $t = 388$ yr. Distances from the grid centre are in au.

ent nature of the disc dynamics that we have used. Some differences between the peak gas phase fractional abundances that we obtained and those reported in other papers are due to the assumptions that we have made about chemical initial conditions. However, the major differences in the chemistry away from the outer boundaries of the disc arise from the role that some other modellers assume that diffusion plays in enhancing the richness of the chemistry in the disc interior (e.g. Ilgner et al. 2004; Heinzel et al. 2011); in many of these models, the chemistry at the midplane is not very rich over a very large fraction of the disc. In contrast, our model gives rise to substantial gas-phase abundances near the midplane, even though we have not assumed that efficient microscopic mixing is a consequence of large-scale turbulence. Though inclusion of such mixing would be difficult in an approach in which individual fluid elements are followed, we have not neglected that type of mixing for that reason. Rather, we have chosen to focus on how gravitational instability generates shocks which induce a rich gas-

phase chemical composition in the disc interior, even near the midplane (see Appendix A).

ALMA will revolutionise observational studies of discs. If used to observe a disc in the Taurus-Auriga cloud complex, ALMA, with its 5 milliarcsec resolution, will allow the mapping of features on scales of about 1 au, which is smaller than the widths of the prominent spiral structures of our model. We plan to use our results in radiative transfer calculations to obtain reliable estimates of the detectability of structure in different species.

ACKNOWLEDGMENTS

We are grateful to Pierre Lesaffre for a thorough and helpful referee’s report. We have benefitted from the use of data in the online database KIDA (KINetic Database for Astrochemistry⁴). Resources supporting the hydrodynamics sim-

⁴ <http://kida.obs.u-bordeaux1.fr>

ulation were provided by the NASA High-End Computing (HEC) Program through the NASA Advanced Supercomputing (NAS) Division at Ames Research Center. JDI gratefully acknowledges a studentship from the Science and Technology Facilities Council of the United Kingdom (STFC). ACB's contribution was supported in part by the National Science Foundation under Grant No. PHY05-51164 and in part under contract with the California Institute of Technology (Caltech) funded by NASA through the Sagan Fellowship Program. PC's and TWH's work on star and planet formation is supported by a STFC rolling grant. RHD was supported in part by NASA Origins of Solar Systems grant NNX08AK36G. TWH appreciates funding provided by the Indiana University Institute for Advanced Study.

REFERENCES

- Aikawa Y., Umebayashi T., Nakano T., Miyama S. M., 1999, *ApJ*, 519, 705
- Aikawa Y., van Zadelhoff G. J., van Dishoeck E. F., Herbst E., 2002, *A&A*, 386, 622
- Armitage P. J., Livio M., Pringle J. E., 2001, *MNRAS*, 324, 705
- Bergin E., Calvet N., D'Alessio P., Herczeg G. J., 2003, *ApJ*, 591, L159
- Boley A. C., 2007, PhD thesis, Indiana University
- Boley A. C., 2009, *ApJ*, 695, L53
- Boley A. C., Durisen R. H., 2008, *ApJ*, 685, 1193
- Boley A. C., Durisen R. H., 2010, *ApJ*, 724, 618
- Boley A. C., Durisen R. H., Nordlund Å., Lord J., 2007a, *ApJ*, 665, 1254
- Boley A. C., Hartquist T. W., Durisen R. H., Michael S., 2007b, *ApJ*, 656, L89
- Boley A. C., Hayfield T., Mayer L., Durisen R. H., 2010, *Icarus*, 207, 509
- Boley A. C., Mejía A. C., Durisen R. H., Cai K., Pickett M. K., D'Alessio P., 2006, *ApJ*, 651, 517
- Boss A. P., 2001, *ApJ*, 563, 367
- Boss A. P., 2007, *ApJ*, 661, L73
- Brown P. N., Byrne G. D., Hindmarsh A. C., 1989, *SIAM Journal on Scientific and Statistical Computing*, 10, 1038
- Cai K., Pickett M. K., Durisen R. H., Milne A. M., 2010, *ApJ*, 716, L176
- Cossins P., Lodato G., Clarke C. J., 2009, *MNRAS*, 393, 1157
- Durisen R. H., Boss A. P., Mayer L., Nelson A. F., Quinn T., Rice W. K. M., 2007, *Protostars and Planets V*, pp 607–622
- Dutrey A., Henning T., Guilloteau S., Semenov D., Piétu V., Schreyer K., Bacmann A., Launhardt R., Pety J., Gueth F., 2007, *A&A*, 464, 615
- Ehrenfreund P., Charnley S. B., 2000, *ARA&A*, 38, 427
- Ehrenfreund P., Schutte W. A., 2000, *Advances in Space Research*, 25, 2177
- Fogel J. K. J., Bethell T. J., Bergin E. A., Calvet N., Semenov D., 2011, *ApJ*, 726, 29
- Gammie C. F., 1996, *ApJ*, 457, 355
- Gammie C. F., 2001, *ApJ*, 553, 174
- Gorti U., Hollenbach D., 2004, *ApJ*, 613, 424
- Guilloteau S., Dutrey A., 2008, *Ap&SS*, 313, 95
- Hasegawa T. I., Herbst E., Leung C. M., 1992, *ApJS*, 82, 167
- Heinzeller D., Nomura H., Walsh C., Millar T. J., 2011, *ApJ*, 731, 115
- Henning T., Semenov D., Guilloteau S., Dutrey A., Hersant F., Wakelam V., Chapillon E., Launhardt R., Piétu V., Schreyer K., 2010, *ApJ*, 714, 1511
- Hollenbach D., Kaufman M. J., Bergin E. A., Melnick G. J., 2009, *ApJ*, 690, 1497
- Ilgner M., Henning T., Markwick A. J., Millar T. J., 2004, *A&A*, 415, 643
- Lodato G., Clarke C. J., 2011, *MNRAS*, pp 333–+
- Lodato G., Rice W. K. M., 2004, *MNRAS*, 351, 630
- Markwick A. J., Ilgner M., Millar T. J., Henning T., 2002, *A&A*, 385, 632
- Mayer L., Lufkin G., Quinn T., Wadsley J., 2007, *ApJ*, 661, L77
- Mayer L., Quinn T., Wadsley J., Stadel J., 2004, *ApJ*, 609, 1045
- Mejía A. C., Durisen R. H., Pickett M. K., Cai K., 2005, *ApJ*, 619, 1098
- Meru F., Bate M. R., 2011, *MNRAS*, 411, L1
- Michael S., Steiman-Cameron T. Y., Durisen R. H., Boley A. C., 2011, *ApJ*, submitted
- Millar T. J., Farquhar P. R. A., Willacy K., 1997, *A&AS*, 121, 139
- Nomura H., Aikawa Y., Nakagawa Y., Millar T. J., 2009, *A&A*, 495, 183
- Nomura H., Millar T. J., 2005, *A&A*, 438, 923
- Öberg K. I., Qi C., Fogel J. K. J., Bergin E. A., Andrews S. M., Espaillat C., van Kempen T. A., Wilner D. J., Pascucci I., 2010, *ApJ*, 720, 480
- Podolak M., Mayer L., Quinn T., 2010, *astro-ph/1012.5269*
- Qi C., Wilner D. J., Aikawa Y., Blake G. A., Hogerheijde M. R., 2008, *ApJ*, 681, 1396
- Schreyer K., Guilloteau S., Semenov D., Bacmann A., Chapillon E., Dutrey A., Gueth F., Henning T., Hersant F., Launhardt R., Pety J., Piétu V., 2008, *A&A*, 491, 821
- Semenov D., Hersant F., Wakelam V., Dutrey A., Chapillon E., Guilloteau S., Henning T., Launhardt R., Piétu V., Schreyer K., 2010, *A&A*, 522, A42+
- Semenov D., Pavlyuchenkov Y., Henning T., Wolf S., Launhardt R., 2008, *ApJ*, 673, L195
- Semenov D., Wiebe D., 2011, *astro-ph/1104.4358*
- Stamatellos D., Hubber D. A., Whitworth A. P., 2007, *MNRAS*, 382, L30
- Toomre A., 1964, *ApJ*, 139, 1217
- Vasyunin A. I., Wiebe D. S., Birnstiel T., Zhukovska S., Henning T., Dullemond C. P., 2011, *ApJ*, 727, 76
- Visser R., van Dishoeck E. F., Doty S. D., Dullemond C. P., 2009, *A&A*, 495, 881
- Vorobyov E. I., Basu S., 2005, *ApJ*, 633, L137
- Vorobyov E. I., Basu S., 2006, *ApJ*, 650, 956
- Vorobyov E. I., Basu S., 2009, *MNRAS*, 393, 822
- Vorobyov E. I., Basu S., 2010, *ApJ*, 714, L133
- Walsh C., Millar T. J., Nomura H., 2010, *ApJ*, 722, 1607
- Willacy K., 2007, *ApJ*, 660, 441
- Willacy K., Klahr H. H., Millar T. J., Henning T., 1998, *A&A*, 338, 995
- Willacy K., Langer W., Allen M., Bryden G., 2006, *ApJ*, 644, 1202
- Woitke P., Thi W., Kamp I., Hogerheijde M. R., 2009,

- A&A, 501, L5
 Woodall J., Agúndez M., Markwick-Kemper A. J., Millar T. J., 2007, A&A, 466, 1197
 Zhu Z., Hartmann L., Gammie C., 2009, ApJ, 694, 1045
 Zhu Z., Hartmann L., Gammie C., 2010, ApJ, 713, 1143
 Zhu Z., Hartmann L., Gammie C. F., Book L. G., Simon J. B., Engelhard E., 2010, ApJ, 713, 1134

APPENDIX A: OTHER PERSPECTIVES

Figure A1 shows the column densities of selected species in the disc as viewed along the y -axis, toward $y = 0$, in Fig. 1. The majority of the edge-on maps show little structure (as with CO and H₂O), though some, such as the H₂CO and SO maps, show slightly higher column densities on the right side due to the presence of a large spiral arm.

Figure A2 shows slices of the fractional abundances in the interior of the disc for HCN and H₂CO. These show little structure in the disc interior when compared with other models of axisymmetric discs. These shock-desorbed molecules show little structure in the disc interior compared with what is seen in axisymmetric α -disc models.

APPENDIX B: THREE-BODY REACTIONS

Table B1 lists the three-body reactions included in the chemical network and taken from Willacy et al. (1998) and the more recent UMIST Database for Astrochemistry, UDfA⁵. The subset includes only the reactions possessing activation energies of less than 10^4 K.

This paper has been typeset from a T_EX/ L^AT_EX file prepared by the author.

⁵ <http://www.udfa.net>

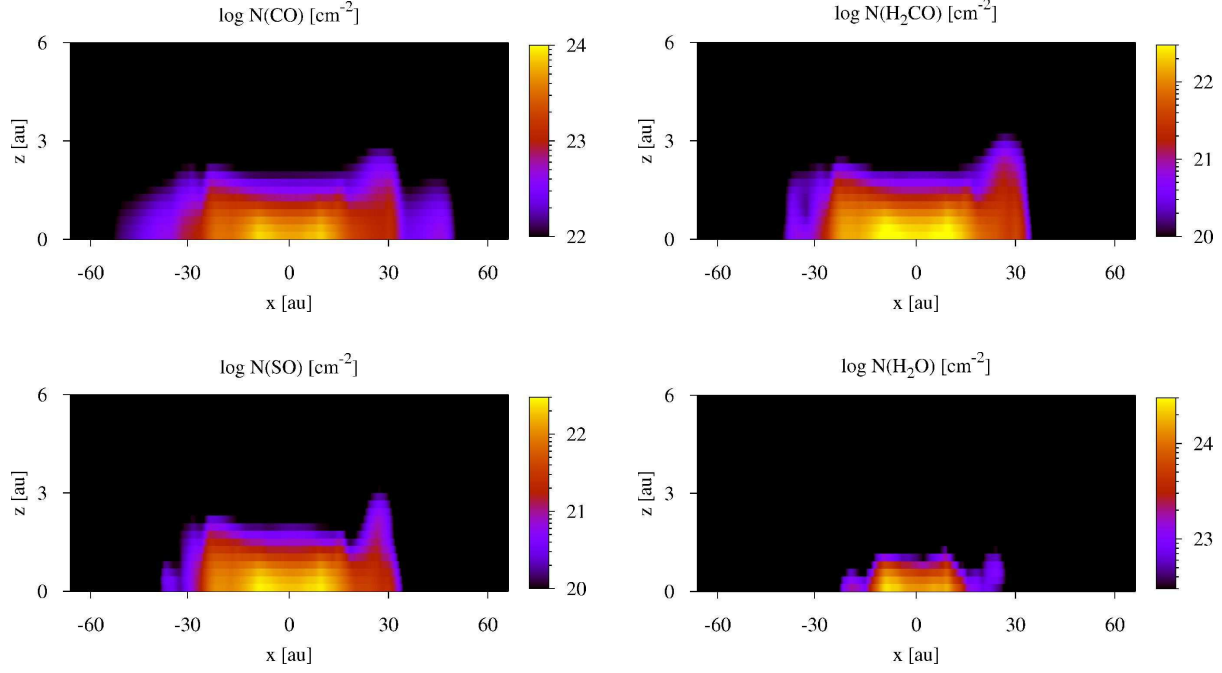


Figure A1. Column densities of the disc as viewed along the y -axis of Fig. 1, towards $y = 0$, at $t = 388$ yr.

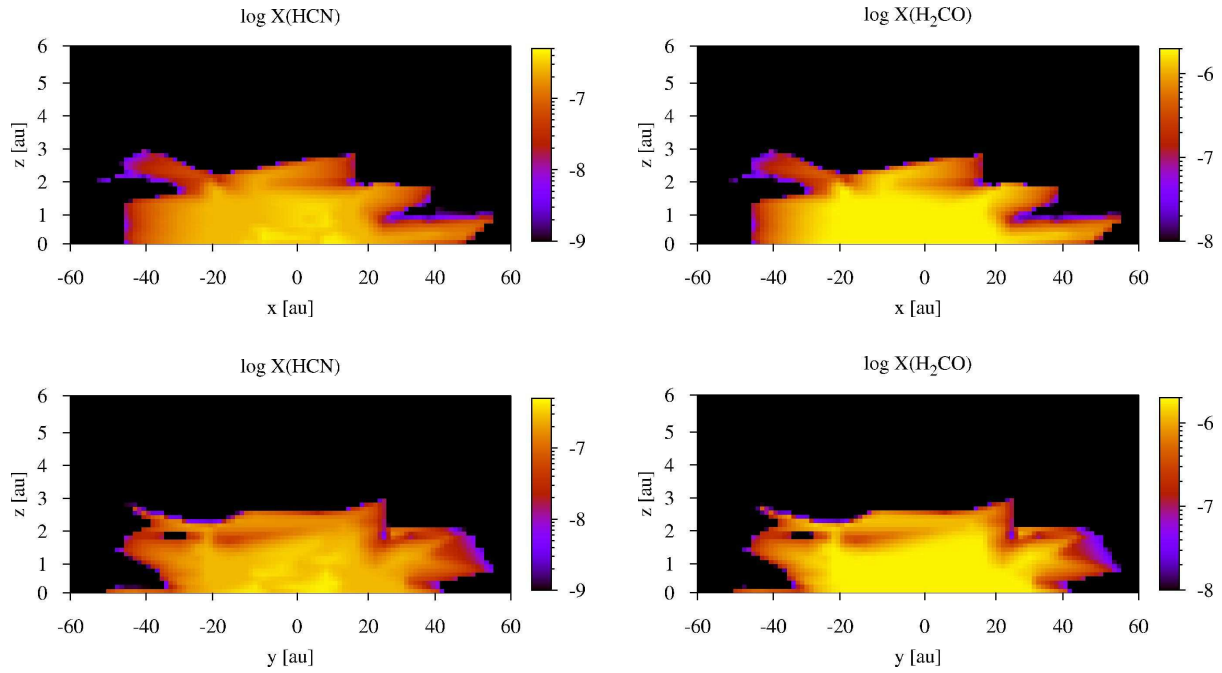


Figure A2. Slices of the fractional abundance of disc interior, oriented as in Figure 4, interpolated from the positions of the fluid elements at $t = 388$ yr.

Table B1. Three-body reactions included in the chemical network. In all but one of the reactions the third body is assumed to be molecular hydrogen. References are W: Willacy et al. (1998) and U: Woodall et al. (2007).

R_1	R_2	R_3	\rightarrow	P_1	P_2	α	β	γ	Reference
CH ₃	H	H ₂	\rightarrow	CH ₄	H ₂	9.62(-31)	-1.80	3231.0	W
N	O	H ₂	\rightarrow	NO	H ₂	3.86(-34)	0.00	2573.0	W
O	O	H ₂	\rightarrow	O ₂	H ₂	5.25(-35)	0.00	902.0	W
O	H	H ₂	\rightarrow	OH	H ₂	6.23(-34)	0.00	1960.0	W
OH	H	H ₂	\rightarrow	H ₂ O	H ₂	6.86(-31)	-2.00	0.0	W
C	O	H ₂	\rightarrow	CO	H ₂	2.14(-29)	-3.08	2441.0	W
CO	O	H ₂	\rightarrow	CO ₂	H ₂	9.56(-34)	0.00	1060.0	W
H	CO	H ₂	\rightarrow	HCO	H ₂	5.30(-34)	0.00	370.0	W
SO	O	H ₂	\rightarrow	SO ₂	H ₂	1.86(-31)	-0.50	0.0	W
H	H	H ₂	\rightarrow	H ₂	H ₂	8.72(-33)	-0.60	0.0	W
H	H	H	\rightarrow	H	H ₂	1.83(-31)	-1.00	0.0	W
N	N	H ₂	\rightarrow	N ₂	H ₂	9.53(-34)	-0.50	0.0	W
N	H	H ₂	\rightarrow	NH	H ₂	3.09(-32)	-0.50	0.0	W
NH	H	H ₂	\rightarrow	NH ₂	H ₂	3.18(-33)	-0.50	0.0	W
NH ₂	H	H ₂	\rightarrow	NH ₃	H ₂	1.32(-33)	0.00	4366.0	W
H	CH ₃	H ₂	\rightarrow	CH ₄	H ₂	6.16(-29)	-1.80	0.0	U
H	O	H ₂	\rightarrow	OH	H ₂	4.33(-32)	-1.00	0.0	U
H	NH ₂	H ₂	\rightarrow	NH ₃	H ₂	6.06(-30)	0.00	0.0	U
H	OH	H ₂	\rightarrow	H ₂ O	H ₂	1.51(-31)	-2.65	1.9	U
H	CO	H ₂	\rightarrow	HCO	H ₂	5.30(-34)	0.00	370.0	U
H	HCO	H ₂	\rightarrow	H ₂ CO	H ₂	3.16(-30)	-2.57	215.0	U
H	NO	H ₂	\rightarrow	HNO	H ₂	1.33(-31)	-1.32	370.0	U
H ₂	C	H ₂	\rightarrow	CH ₂	H ₂	7.00(-32)	0.00	0.0	U
H ₂	CH	H ₂	\rightarrow	CH ₃	H ₂	3.79(-30)	-1.84	65.4	U
H ₂	N	H ₂	\rightarrow	NH ₂	H ₂	1.00(-26)	0.00	0.0	U
C	N	H ₂	\rightarrow	CN	H ₂	9.41(-33)	0.00	0.0	U
O	SO	H ₂	\rightarrow	SO ₂	H ₂	9.15(-31)	-1.84	0.0	U
O	O	H ₂	\rightarrow	O ₂	H ₂	1.98(-34)	-0.48	-564.0	U
C	O	H ₂	\rightarrow	CO	H ₂	2.14(-29)	-3.08	-2114.0	U
C ⁺	O	H ₂	\rightarrow	CO ⁺	H ₂	2.14(-27)	-3.08	-2114.0	U
C	O ⁺	H ₂	\rightarrow	CO ⁺	H ₂	2.14(-27)	-3.08	-2114.0	U
C	C	H ₂	\rightarrow	C ₂	H ₂	1.26(-32)	-0.64	-5255.0	U